IEEE Photonics Journal
An IEEE Photonics Society Publication

Thermoelectric Effect in Quantum Cascade Lasers

Volume 2, Number 3, June 2010

Matthew D. Escarra, Student Member, IEEE
Alexander Benz
Anjali M. Bhatt
Anthony J. Hoffman
Xiaojun Wang
Jen-Yu Fan
Claire Gmachl

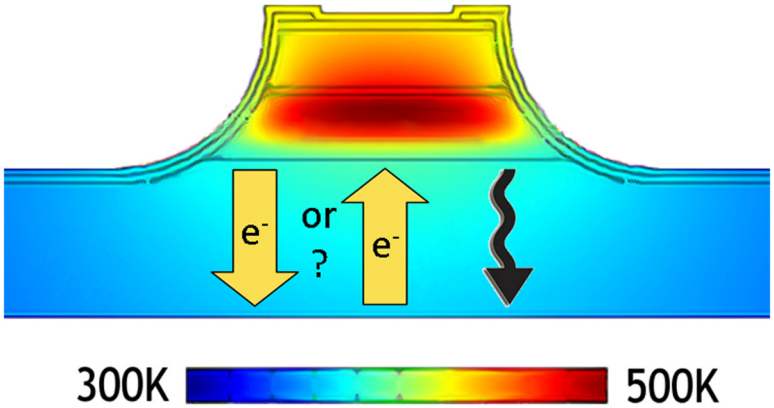

DOI: 10.1109/JPHOT.2010.2050304
1943-0655/$26.00 ©2010 IEEE

Thermoelectric Effect in Quantum Cascade Lasers

Matthew D. Escarra,[1] *Student Member, IEEE*, Alexander Benz,[1,2] Anjali M. Bhatt,[1,3] Anthony J. Hoffman,[1] Xiaojun Wang,[4] Jen-Yu Fan,[4] and Claire Gmachl[1]

[1]Department of Electrical Engineering, Princeton University, Princeton, NJ 08544 USA
[2]Photonics Institute, Vienna University of Technology, 1040 Vienna, Austria
[3]Department of Physics, Harvard University, Cambridge, MA 02138 USA
[4]AdTech Optics, Inc., City of Industry, CA 91748 USA

DOI: 10.1109/JPHOT.2010.2050304
1943-0655/$26.00 ©2010 IEEE

Manuscript received March 29, 2010; revised May 6, 2010; accepted May 6, 2010. Date of publication May 12, 2010; date of current version June 11, 2010. This work was supported in part by DARPA-EMIL, by MIRTHE (NSF-ERC #EEC-0540832), and by REU Site: I-MIRTHE REU (#EEC-0648721).
Corresponding author: M. D. Escarra (e-mail: escarra@princeton.edu).

Abstract: The choice of polarity of operation in a quantum cascade (QC) laser is made at the beginning of every QC laser design and growth, yet little work has been done to ascertain any performance benefits of one polarity versus the other. In this paper, we compare two QC lasers of the same design, differentiated only by the reversing of the growth order of the heterostructure layers in the laser core, which results in opposite polarities of operation. Analysis is performed through continuous wave (CW) and pulsed threshold current measurements to observe the change in active core temperature with input power. A thermoelectric effect is observed, where the direction of current flow improves thermal transport in negative polarity lasers (electron flow toward the heat sink) over positive polarity (electron flow away from the heat sink), leading to a maximum observed reduction in laser core heating of 10.0 ± 5.5 K for a thermal load of 7.2 kW/cm^2 in CW operation.

Index Terms: Quantum cascade lasers, thermoelectric effect, superlattice devices, optoelectronic materials, thermal modeling.

1. Introduction

Quantum cascade (QC) lasers, as superlattices composed of numerous quantum wells, have an innately large design space [1]. These devices employ band structure engineering to achieve a broad array of highly desirable performance characteristics across a wide range of emission wavelengths in both the infrared and terahertz portions of the electromagnetic spectrum [2]–[5]. This broad flexibility makes the lasers excellent candidates for sensing applications ranging from breath diagnostics to industrial and environmental monitoring. Yet, beyond the pure electronic and photonic effects of band structure engineering, superlattice structures are known to show other unique properties [6]–[8], some of which have yet to be exploited in optimizing QC laser performance. For example, semiconductor superlattices have been demonstrated to show a thermoelectric response that is an order of magnitude higher than that of bulk semiconductor materials [9], [10]. As superlattice-like devices, QC lasers can be expected to also show this enhanced thermoelectric effect. Previously, thermoelectric cooling has been modeled in the active core of bipolar semiconductor lasers [11]. Here, we seek to determine if there is a measurable thermoelectric effect occurring in QC lasers, and if so, how it can best be used to improve laser performance. A potential thermoelectric effect is of particular interest due to its likely impact on the

lasers' core temperature in continuous wave (CW) operation, as the effect plays an important role in heat transport through the superlattice-like core. QC laser performance is highly dependent on the temperature of this core, with performance decreasing as core temperature increases; any method of reducing the core temperature that does not sacrifice performance in any other way would therefore be highly valuable.

In order to study a possible thermoelectric effect in QC lasers and its effect on core temperature, two QC structures are designed and fabricated, where the only difference between the two is in their polarity of operation with respect to the location of the heat sink. With a given quantum design, the choice of growth order, fabrication method, and mounting orientation (epitaxial-side up versus down) all play a role in determining the polarity with which the device will operate. Here, the growth order is reversed from one structure to the other so that one operates with a positive voltage bias on the top contact, while the other operates with a negative bias on the top contact. By changing the growth order and subsequent polarity of operation, the direction of current flow is changed, causing a reversal of any thermoelectric effect which can then be measured.

Previous studies concerning positive and negative biasing of QC lasers have focused on bidirectional devices, where the same laser emits light under both polarities [12]. Here, we are considering only unidirectional devices, where the device is designed for light emission under only one polarity: positive or negative. The device polarity is defined as the sign of the voltage bias applied to the top electrical contact of the device. Thus, for the same QC laser, the polarity of operation flips only when the laser flips from epitaxial-side up mounting to epitaxial-side down mounting.

2. Thermoelectric Model

The thermoelectric effect is the direct coupling of a voltage difference with a temperature difference in a medium. The effect harnesses the thermal nature of charge carriers, where electrons (or holes) serve to transport heat in their direction of propagation. This is in addition to the conventional method of heat transport through the crystal via phonons.

In order to properly understand the impact of the thermoelectric effect on QC laser performance, a coupled thermal and electrical transport model was developed. The thermoelectric effect is described by a system of coupled differential equations [13]:

$$\boldsymbol{J} = -\sigma \cdot \nabla \boldsymbol{V} - \sigma \cdot S \cdot \nabla \boldsymbol{T} \tag{1}$$

$$\boldsymbol{Q} = -\sigma \cdot S \cdot T \cdot \nabla \boldsymbol{V} - (\sigma \cdot S^2 \cdot T + \kappa) \cdot \nabla \boldsymbol{T} \tag{2}$$

where the electric current density $\boldsymbol{J}$, heat flux $\boldsymbol{Q}$, electric potential $\boldsymbol{V}$, and temperature $\boldsymbol{T}$ are vector quantities. The electrical conductivity σ and thermal conductivity κ are temperature dependent and anisotropic in some cases, as detailed below. The Seebeck coefficient S determines the strength of the thermoelectric effect. Based on these equations, we use a commercial software package (COMSOL Multiphysics) that employs the finite element method to calculate the temperature and electrical current distribution over a 2-D cross section of the laser geometry. The modeled geometry is an epitaxial-side up mounted ridge laser with only a "thin-gold" top contact. This structure is chosen for accurate comparison with our experimentally measured devices, which are processed in the same manner.

The Seebeck coefficients used in the model for the InP substrate and waveguide $(5 \times 10^{-4}$ V/K$)$ [14] and the InGaAs cladding and contact layers $(4 \times 10^{-4}$ V/K$)$ [9] are bulk material characteristics taken from literature. The Seebeck coefficient chosen for the active region $(2 \times 10^{-3}$ V/K is based on previously studied superlattices of similar thickness composed of InGaAs and AlInAs [9], [10].

As for thermal properties, a temperature dependent thermal conductivity was used for the InP substrate and waveguide layers [15] and InGaAs waveguide layers [16]. The thermal conductivity values used for the SiO_2 insulating layer and the gold contact were 10 W/m · K and 320 W/m · K, respectively. For the active core, the thermal conductivity was considered to be anisotropic, where the in-plane thermal conductivity $\kappa_{\parallel}$ (5 W/m · K) is higher than the out-of-plane $\kappa_{\perp}$ (1 W/m · K) [17]. The thermal conductivity is lower in the growth direction because several hundred interface layers

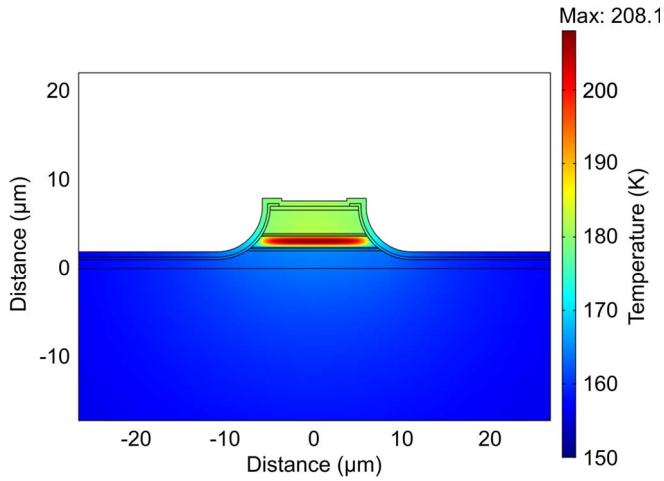

Fig. 1. Temperature distribution over the cross section of a QC laser ridge calculated using the finite-element method. The modeled ridge geometry corresponds to a laser that is fabricated with "thin-gold" top contacts mounted epitaxial-side up, operated in CW mode with 19.9 kW/cm^2 of input power density. The model incorporates the thermoelectric effect and shows a maximum core temperature of 208.1 K for a negatively biased laser with heat sink temperature of 150 K. The same model shows a maximum core temperature of 211.5 K for a positively biased laser.

serve to impede heat transport. Nevertheless, a model including this anisotropy shows a very small difference in the heating of the core and the thermoelectric effect, as compared with a model employing an isotropic thermal conductivity of 1 W/m · K [17].

For the electrical transport aspect of the model, a temperature and doping dependent electrical conductivity was used for all of the InP and InGaAs substrate and waveguide layers [15]. The electrical conductivity for the thin SiO_2 insulator and gold contact was $1 \times 10^{-6}\ (\Omega \cdot \mathrm{m})^{-1}$ and $5.8 \times 10^{7}\ (\Omega \cdot \mathrm{m})^{-1}$, respectively. For the active core, an isotropic electrical conductivity is used, equivalent to that in the cross-plane direction. These devices are deep etched so that current flow through the active core is essentially uniaxial in the cross-plane direction; the net in-plane current flow is negligible. The electrical conductivity for the active core is derived from experimental current–voltage curves, where resistivity versus electric field, for each heat sink temperature, is extracted from the corresponding data of devices used in this study. The experimentally measured threshold voltage is used in the model as the top contact bias voltage. This results in the model also using the same threshold current density and input power density as seen experimentally.

We model this QC laser at a heat sink temperature of 150 K, which is the highest temperature at which the lasers used in this study lased in CW operation. The model shows that the maximum temperature of the active core in CW operation is 208.1 K when negatively biased with 19.9 kW/cm^2 of input power density, as shown in Fig. 1. Conversely, when biased under the same conditions but with positive polarity on the top contact, the maximum temperature in the core rises to 211.5 K, revealing a polarity-dependent temperature reduction of 3.4 K in the core from positive polarity to negative polarity, due to the thermoelectric effect.

3. Laser Design and Fabrication

In order to experimentally quantify this thermoelectric effect, we grew two wafers of the exact same quantum and waveguide design. These wafers were grown back-to-back by metal–organic chemical vapor deposition (MOCVD), with the only difference being that the order of the heterostructure layers in the active core were reversed from one wafer to the other. Thus, the same design requires negative bias for operation in one wafer and positive bias in the other wafer.

The quantum design used here is similar to that of our previous work [18], featuring a low-voltage defect and short, four-quantum-well injector. This design also employs indirect injection from the

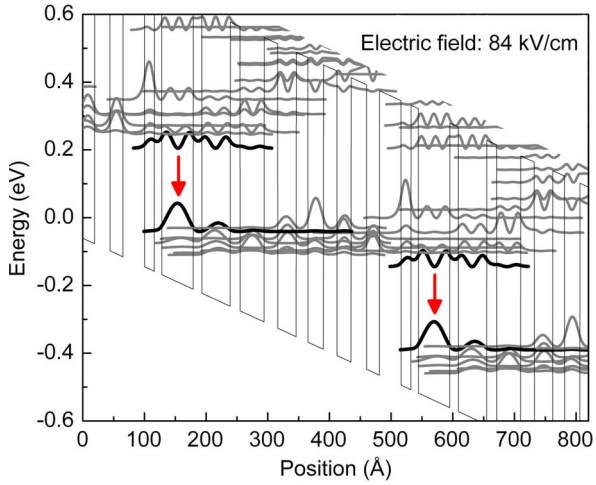

Fig. 2. A portion of the conduction band structure along with the moduli squared of the relevant wave functions. Wave functions in bold illustrate the upper and lower laser levels of each active period. The optical transition, with a design energy of 246 meV, is depicted by vertical arrows. This design features a short (four-quantum-well) injector, a low-voltage defect (80 meV at threshold), and indirect injection from the injector to the upper laser level. The band structure shown is for an applied electric field of 84 kV/cm.

injector to the upper laser level [19]. The layer thicknesses in angstroms in one period of the core, starting from the first well in the injector and continuing in the direction of electron flow, are 30/**19**/25/**22**/23/**25**/21/**35**/16/**12**/51/**14**/46/**16**/39/**22**, where $In_{0.653}Ga_{0.347}As$ well layers are plain, $In_{0.33}Al_{0.67}As$ barrier layers are bold, and the n-doped (1×10^{17} cm^{-3}) layers are underlined. A portion of the conduction band is shown in Fig. 2. Both wafers consist of 30 periods of active/injector regions, sandwiched between two lattice-matched 0.14-μm thick $In_{0.53}Ga_{0.47}As$ optical confinement layers (n-doped 0.2×10^{17} cm^{-3}). A 2-μm buffer layer of InP (0.2×10^{17} cm^{-3}) was initially grown on the InP substrate before the first confinement layer. Additional top cladding layers of 2.67-μm InP (0.2×10^{17} cm^{-3}), 0.43-μm InP (80×10^{17} cm^{-3}), and finally, 0.1-μm $In_{0.53}Ga_{0.47}As$ (2×10^{19} cm^{-3}) were grown. In total, the active region is 1.25 μm thick, and the epitaxial layer is 6.81 μm thick.

Devices from both wafers were fabricated together as deep-etched ridge waveguide lasers of varying widths with SiO_2 (3000 Å) for side-wall electrical insulation. The devices were thinned to ~200 μm and Ti/Au (200 Å/6000 Å) top contacts and Ge/Au (200 Å/3000 Å) bottom contacts were deposited by electron-beam evaporation. Some of the devices from each polarity were annealed at 400 °C for 30 seconds. Ridges were cleaved to 1.5 mm in length and mounted epitaxial-side up on copper heat sinks, with each heat sink having a positive and negative polarity ridge of practically equal width mounted side by side. Careful attention was taken throughout the growth and fabrication process to assure that a thorough comparison could be made between devices from the two polarities.

4. Experimental Results and Discussion

X-ray diffraction spectra were taken of both the positive and negative polarity wafers before processing (see Fig. 3). These diffraction spectra have significant overlap and show good wafer quality for both wafers; they indicate no major structural differences between the two wafers due to the reversal of growth order.

In order to further compare the wafers' band structures, electroluminescence measurements were made on cleaved mesas at 80 K with 400 mA of current. This electroluminescence data also show good agreement in the spectral shape. The negative polarity peak is centered at 248 meV with a full-width at half-maximum (FWHM) of 6% of the peak energy. Similarly, the positive polarity peak is centered at 252 meV with a FWHM of 5% of the peak energy. Spectral measurements were also made on 1.5-mm-long laser ridges at 80 K under pulsed operation, as seen in the inset of

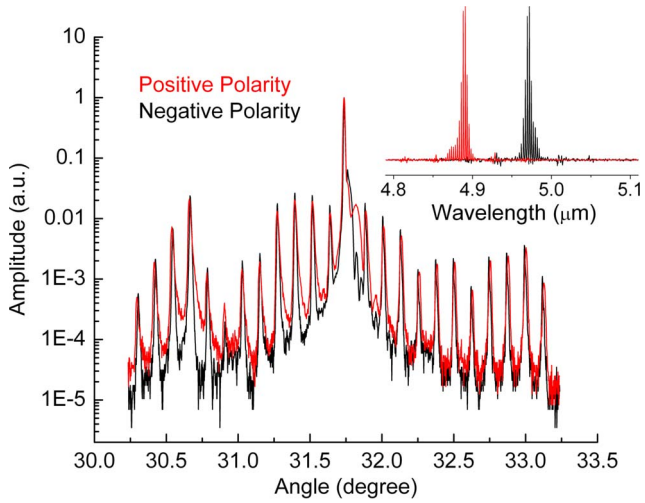

Fig. 3. X-ray diffraction spectra are shown for both wafers in this study, confirming that both wafer growths are of good quality with little structural difference. The inset shows two laser spectra: one for a device fabricated from each wafer. These spectra are taken at 80 K under pulsed operation with current that is 10% above threshold.

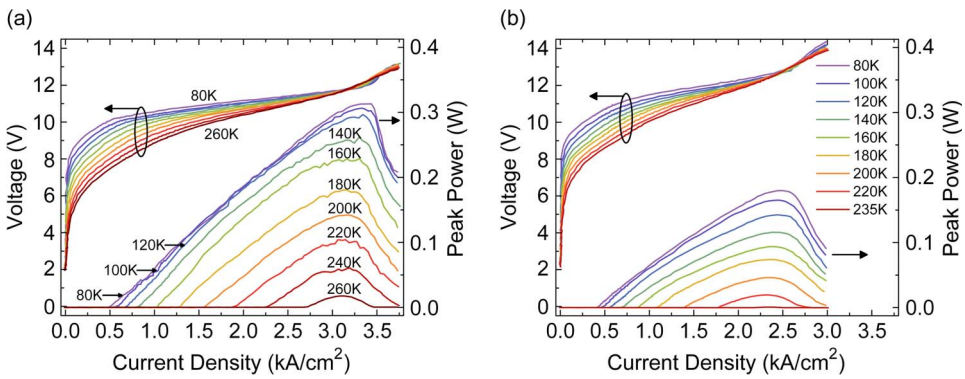

Fig. 4. (a) Pulsed LIV measurements for a 1.5-mm-long and 10.2-μm-wide laser ridge at the indicated heat sink temperatures, operating under negative bias. The pulse width is 100 ns, and the frequency is 5 kHz, resulting in a 0.05% duty cycle. (b) Similarly, pulsed LIV measurements are shown for a 1.5-mm-long and 10.8-μm-wide laser ridge operating under positive bias. The light in each of these plots is corrected for a collection efficiency of 75%.

Fig. 3. The negative polarity laser has a center wavelength of 4.97 μm; the positive polarity laser has a center wavelength of 4.89 μm, again showing similar performance.

Light–current–voltage (LIV) measurements were performed on many different lasers of both polarities in both pulsed and CW mode. Fig. 4(a) depicts the temperature-dependent pulsed LIV characteristics of a 1.5-mm-long and 10.2-μm-wide laser ridge from the negative polarity wafer. Fig. 4(b) shows the LIV characteristics of a similar sized (1.5 mm by 10.8 μm) positive polarity laser in pulsed operation. These lasers show characteristics representative of what was seen over many other pairs of matched ridges. Thresholds are low, as expected with a short injector design, with threshold densities at 80 K around 0.42 kA/cm^2 for a 1.5-mm-long device and 0.24 kA/cm^2 for a 3-mm-long device. These low temperature threshold current densities are close to the lowest values reported to date in QC lasers [20], [21]. Devices also show low voltage defect operation, as designed, with a voltage defect at 80 K around 77 meV and 86 meV for negative and positive polarity, respectively. There are some other noticeable performance differences between the polarities. Negative polarity lasers have around 10%–20% higher threshold current density than positive

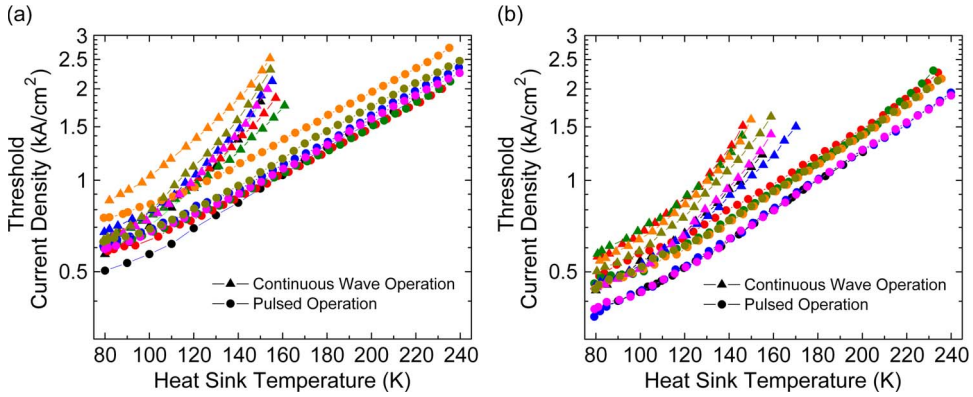

Fig. 5. Threshold current density is plotted versus heat sink temperature in both CW (triangles) and pulsed (circles) operation for both (a) negatively biased and (b) positively biased lasers. Data from seven devices are plotted for each wafer, all with ridge length of 1.5 mm. Ridge widths range from 8 to 14 μm, with positive and negative ridges of equal width (shown in the same color) mounted on the same copper heat sink and measured together.

polarity lasers, but they also have about 30% higher maximum current density (J_{max}). Negative-polarity lasers also show lower differential resistance, slightly lower turn-on voltage, and slightly higher slope efficiency. All of these differences point to a higher free carrier doping density in the injector for the negative polarity wafer, with the difference in doping density between the two wafers being proportional to the difference in J_{max} between positive and negative polarity devices. Due mainly to the much higher J_{max} and a larger dynamic range in current, negative-polarity lasers show much higher peak output power. In addition, the average pulsed characteristic temperature $(T_0 = 109\ \text{K})$ for negative polarity is higher than that for positive polarity $(T_0 = 90\ \text{K})$, where T_0 is calculated from fitting the threshold current density versus heat sink temperature curve to an exponential of the form $J_{th} = J_0 \exp(T/T_0)$.

In order to characterize the temperature performance, threshold current density measurements were taken across a broad range of heat sink temperatures under both CW and pulsed operation for many devices of both polarities. Threshold current densities for seven exemplary devices from each polarity, with length 1.5 mm and widths ranging from 8 to 14 μm, are shown in Fig. 5(a) and (b). These lasers were measured in pairs by examining matching width devices on the same copper block. The threshold current density for a laser in CW mode was compared with the same threshold current density for the same laser under pulsed mode; the active core temperature of the CW measurement is considered to be the same as the heat sink temperature of the pulsed measurement with the same threshold current density. This determination of the active core temperature in CW operation assumes that there is no heating of the core in a pulsed measurement beyond the heat sink temperature, and that the threshold is consistent across the same core temperature. By this method, one can extract the total heating of the active core in CW operation over all of the heat sink temperatures measured. This analysis was performed on all of the lasers shown in Fig. 5(a) and (b). The results are shown in Fig. 6(b), where the core temperature increase $(\Delta T = T_{core} - T_{sink})$ is plotted versus input power density. The input power density is the threshold current density multiplied by the threshold voltage in CW mode and is converted almost entirely into thermal energy dissipated in the active core at threshold. By comparing the amount of core heating for a given input power density (i.e., thermal load), where the only difference between devices is the direction of current flow, one can measure any thermoelectric effect. Indeed, as seen in Fig. 6(a), a measurable thermoelectric effect is occurring in these QC lasers. This effect is especially apparent at lower thermal loads, where the average reduction in core heating due to the thermoelectric effect is 10.0 ± 5.5 K for a thermal load of 7.2 kW/cm^2. This effect is reduced at higher thermal loads. One possible reason for this decline is a temperature dependence in the Seebeck coefficient of the active region. In any case, the thermoelectric effect is evident across a broad range of thermal loads, ranging up to 15 kW/cm^2 in these measurements.

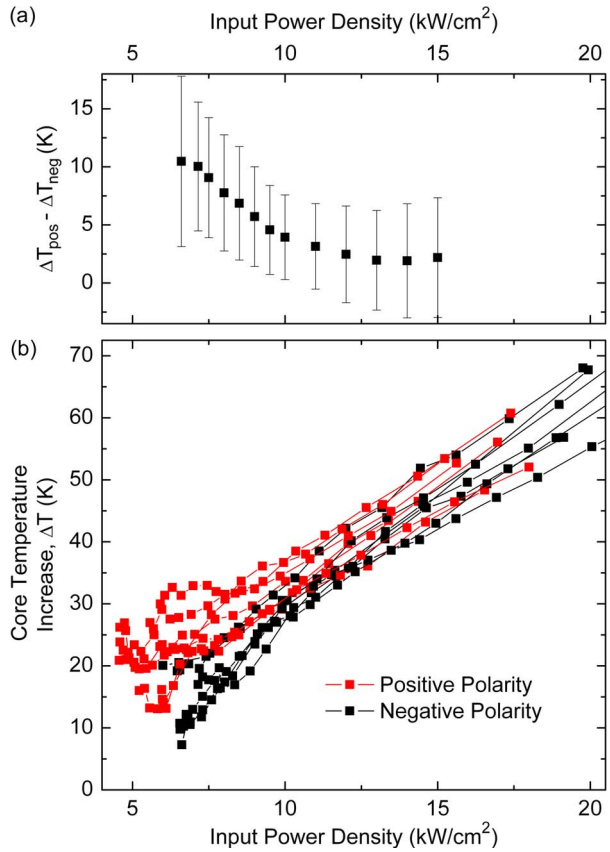

Fig. 6. The core temperature increase $(\Delta T = T_{\text{core}} - T_{\text{sink}})$ is shown versus input electrical power density (i.e., thermal load) for 14 lasers—seven of positive polarity (red) and seven of negative polarity (black). The core temperature is derived from the threshold current measurements shown in Fig. 5, when the input power is still entirely converted into heat. A small thermoelectric effect is apparent, where the device polarity affects the magnitude of heating in the laser active core for a given thermal load. (a) The difference between the average of ΔT for positive polarity and the average of ΔT for negative polarity is shown versus input power density, along with error bars for the measurement. (b) Plot of core temperature increase versus input power density.

When comparing these results with the model, there is good agreement in the sign of the effect, where negative polarity devices show reduced core temperature when compared with positive polarity devices under the same thermal load. There is also good agreement in the magnitude of the effect, with both model and experiment showing a thermoelectric core temperature reduction of several degrees Kelvin. However, the model requires a strong temperature dependence in the Seebeck coefficient in order to accurately predict the temperature dependence of the experimental results. This Seebeck coefficient ranges from 38×10^{-3} V/K at 6.6 kW/cm^2 (corresponding roughly to 100 K heat sink temperature) to 2×10^{-3} V/K at 15 kW/cm^2 (roughly 150 K heat sink temperature); these are values that are similar to or within an order of magnitude higher than those seen in literature. Since the Seebeck coefficient for a QC superlattice (and its behavior with temperature) is not known, the model and literature have only limited use for comparison with these experiments versus temperature. Yet, the existence of a thermoelectric effect to reduce laser core temperature by several Kelvin is clear in both model and experiment.

Given the strong dependence on core temperature in both the threshold current and the output light slope efficiency in CW operated QC lasers, especially at high temperatures, utilizing this thermoelectric reduction of the core temperature will improve device performance. This benefit is compounded by a feedback loop, where a reduction in threshold leads to less input heat and an increase in slope efficiency leads to more power efficiency.

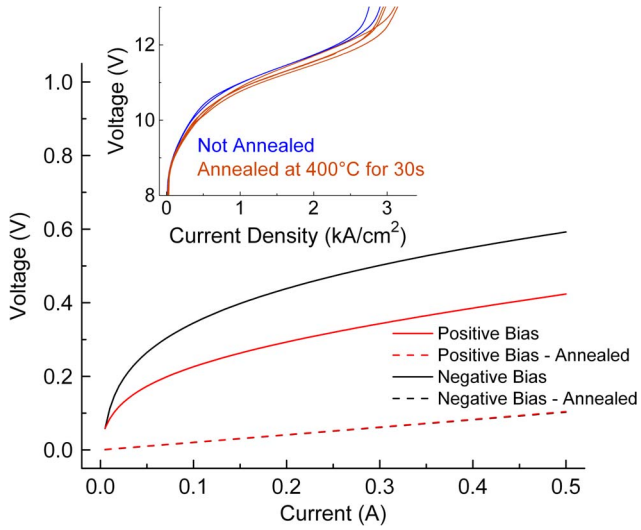

Fig. 7. Current versus voltage characteristics are shown for an "empty" structure, consisting of a QC laser structure without an active core, operated under both negative and positive polarity. When annealed, the voltage across the empty structure drops (positive and negative bias dashed curves lie on top of each other). The inset shows the effect of annealing a conventional QC laser, where the voltage across the contacts is reduced. This voltage reduction is small compared to the total voltage dropped across the lasers.

5. Experimental Analysis of Electrical Contacts

Since we are measuring the thermoelectric effect through polarity dependent measurements of core heating, we must also consider the polarity dependence of the contacts and any additional heating they might contribute. In our structures, the top metal–semiconductor junction is ohmic. This is achieved by using a degenerately doped $(2 \times 10^{19}\ \mathrm{cm}^{-3})$ InGaAs contact layer as the top grown layer, before depositing a Ti/Au top metal contact, as explained earlier. The bottom contact, however, is composed of a low-doped $(1 \times 10^{17}\ \mathrm{cm}^{-3})$ InP substrate with a Ge/Au contact. If not annealed, this contact is not ohmic and requires a turn-on voltage to pass current in both polarities.

In order to quantify the voltage drop across our waveguide and contacts, we took current–voltage (I–V) measurements of an "empty" structure. This "empty" structure is fabricated from a grown wafer consisting of all of the layers typically found in a QC laser wafer, with the exception of the active core heterostructure. In other words, the "empty" wafer has the same substrate, waveguide, confinement, and contact layers as our conventional QC growths. We then fabricated round mesa structures from this wafer using conventional Ti/Au top and Ge/Au bottom contacts. Current–voltage measurements were taken at room temperature in CW mode under both positive and negative polarity. A four-probe measurement technique was used to eliminate any lead resistance from the measurement. The results of these measurements can be seen in Fig. 7. One can see that the negative polarity device has a voltage drop of 0.59 V at 0.5 A, while the positive polarity device has a voltage of 0.42 V at 0.5 A. However, when both devices are annealed at 420 °C for 30 s, the voltage is reduced to 0.1 V at 0.5 A in both devices (red and blacked dashed lines overlap in Fig. 7). This total voltage drop over the "empty" structure in both polarities is very small relative to the total voltage dropped across a conventional QC laser. This can be seen in the inset of Fig. 7, where conventional QC laser I–V curves are shown for both non-annealed and annealed devices. In these QC lasers, the voltage reduction due to annealing the contacts is small (0.2–0.3 V), compared with the total voltage over the device (11–12 V). Furthermore, the contact-related input power is being dissipated as heat mostly at the bottom contact, ~200 μm away from the active core. Thus, the voltage drop across the contacts is small, far from the active core, and shows only ~0.2 V difference between positive and negative polarity, allowing us to conclude that the reduction in heating from positive to negative polarity shown in Fig. 6 is indeed due to a thermoelectric effect and not the contacts.

6. Conclusion

The nature of QC lasers as superlattice-based devices endows them with several unique and advantageous properties. One of these is an enhanced thermoelectric effect, where the direction of current flow can either aid or inhibit heat removal from the active core. This effect is modeled using a coupled thermal and electrical transport model, revealing that choosing the proper polarity of operation can reduce the core temperature by several degrees Kelvin. This effect is then measured in QC lasers, where two sets of lasers of opposing polarity are analyzed side-by-side. The resulting data show a thermoelectric effect in these QC lasers, providing a maximum observed reduction of 10.0 ± 5.5 K in laser core heating from positive to negative polarity, for an input power density of 7.2 kW/cm^2. Furthermore, any polarity-dependence in the contacts was shown to have no impact on this thermoelectric effect. In these epitaxial-side-up mounted devices, the thermoelectric effect provides improved performance when electrons are flowing toward the heat sink (negative polarity growth), as opposed to away from the heat sink (positive polarity growth).

Acknowledgment

The authors would like to acknowledge the contributions of S. S. Howard and K. J. Franz during the early stages of this work.

References

[1] J. Faist, F. Capasso, D. L. Sivco, C. Sirtori, A. L. Hutchinson, and A. Y. Cho, "Quantum cascade laser," *Science*, vol. 264, no. 5158, pp. 553–556, Apr. 1994.
[2] A. Lyakh, C. Pflügl, L. Diehl, Q. J. Wang, F. Capasso, X. J. Wang, J. Y. Fan, T. Tanbun-Ek, R. Maulini, A. Tsekoun, R. Go, and C. K. N. Patel, "1.6-W high wall plug efficiency, continuous-wave room temperature quantum cascade laser emitting at 4.6-μm," *Appl. Phys. Lett.*, vol. 92, no. 11, p. 111 110, Mar. 2008.
[3] J. S. Yu, S. Slivken, A. Evans, and M. Razeghi, "High-performance, continuous-wave quantum-cascade lasers operating up to 85 °C at $\lambda \sim 8.8$ μm," *Appl. Phys. A, Solids Surf.*, vol. 93, pp. 405–408, 2008.
[4] B. G. Lee, H. A. Zhang, C. Pflügl, L. Diehl, M. A. Belkin, M. Fischer, A. Wittman, J. Faist, and F. Capasso, "Broadband distributed-feedback quantum cascade laser array operating from 8.0 to 9.8 μm," *IEEE Photon. Technol. Lett.*, vol. 21, no. 13, pp. 914–916, Jul. 2009.
[5] S. Kumar, Q. Hu, and J. L. Reno, "186 K operation of terahertz quantum-cascade lasers based on a diagonal design," *Appl. Phys. Lett.*, vol. 94, no. 13, p. 131 105, Mar. 2009.
[6] J. P. André, A. Deswarte, E. Lugagne-Delpon, P. Voisin, and P. Ruterana, "High electron mobility in $(InAs)_n(GaAs)_n$ short period superlattices grown by MOVPE for high-electron mobility transistor structure," *J. Electron. Mater.*, vol. 23, no. 2, pp. 141–146, Feb. 1994.
[7] M. Hosoda and S. Noma, "Formation of electric-field domains in a system of multiple finite superlattices," *Phys. Rev. B, Condens. Matter*, vol. 75, no. 20, p. 205 333, May 2007.
[8] Y. A. Romanov, J. Y. Romanova, and L. G. Mourokh, "Electron Bloch oscillations and electromagnetic transparency of semiconductor superlattices in multi-frequency electric fields," *Phys. Rev. B, Condens. Matter*, vol. 79, no. 24, p. 245 320, Jun. 2009.
[9] D. Vashaee and A. Shakouri, "Electronic and thermoelectric transport in semiconductor and metallic superlattices," *J. Appl. Phys.*, vol. 95, no. 3, pp. 1233–1245, Feb. 2004.
[10] J. M. O. Zide, D. Vashaee, Z. X. Bian, G. Zeng, J. E. Bowers, A. Shakouri, and A. C. Gossard, "Demonstration of electron filtering to increase the Seebeck coefficient in $In_{0.53}Ga_{0.47}As/In_{0.53}Ga_{0.28}Al_{0.19}As$ superlattices," *Phys. Rev. B, Condens. Matter*, vol. 74, no. 20, p. 205 335, Nov. 2006.
[11] K. P. Pipe, R. J. Ram, and A. Shakouri, "Bias-dependent Peltier coefficient and internal cooling in bipolar devices," *Phys. Rev. B, Condens. Matter*, vol. 66, no. 12, p. 125 316, Sep. 2002.
[12] C. Gmachl, A. Tredicucci, D. L. Sivco, A. L. Hutchinson, F. Capasso, and A. Y. Cho, "Bidirectional semiconductor laser," *Science*, vol. 286, no. 5440, pp. 749–752, Oct. 1999.
[13] J. P. Troadec and D. Bideau, "Thermoelectric power and percolation," *J. Phys. C, Solid State Phys.*, vol. 16, no. 7, pp. 1169–1177, Mar. 1983.
[14] O. Madelung, U. Rossler, and M. Schulz, *Group IV Elements, IV–IV and III–V Compounds. Part B—Electronic, Transport, Optical and Other Properties*. Berlin, Germany: Springer-Verlag, 2002.
[15] S. Adachi, *Handbook on Physical Properties of Semiconductors, Vol. 1–3*. Berlin, Germany: Springer-Verlag, 2004.
[16] C. Gmachl, A. M. Sergent, A. Tredicucci, F. Capasso, A. L. Hutchinson, D. L. Sivco, J. N. Baillargeon, S. N. G. Chu, and A. Y. Cho, "Improved CW operation of quantum cascade lasers with epitaxial-side heat-sinking," *IEEE Photon. Technol. Lett.*, vol. 11, no. 11, pp. 1369–1371, Nov. 1999.
[17] S. S. Howard, Z. Liu, D. Wasserman, A. J. Hoffman, T. S. Ko, and C. F. Gmachl, "High-performance quantum cascade lasers: Optimized design through waveguide and thermal modeling," *IEEE J. Sel. Topics Quantum Electron.*, vol. 13, no. 5, pp. 1054–1064, Sep./Oct. 2007.

[18] M. D. Escarra, A. J. Hoffman, K. J. Franz, S. S. Howard, R. Cendejas, X. Wang, J.-Y. Fan, and C. Gmachl, "Quantum cascade lasers with voltage defect of less than one longitudinal optical phonon energy," *Appl. Phys. Lett.*, vol. 94, no. 25, p. 251 114, Jun. 2009.
[19] M. Yamanishi, K. Fujita, T. Edamura, and H. Kan, "Indirect pump scheme for quantum cascade lasers: Dynamics of electron-transport and very high T_0-values," *Opt. Express*, vol. 16, no. 25, pp. 20 748–20 758, Dec. 2008.
[20] S. Katz, G. Boehm, and M.-C. Amann, "Low-threshold injectorless quantum cascade laser with four material compositions," *Electron. Lett.*, vol. 44, no. 9, pp. 580–581, Apr. 2008.
[21] S. Katz, A. Vizbaras, G. Boehm, and M.-C. Amann, "High-performance injectorless quantum cascade lasers emitting below 6 μm," *Appl. Phys. Lett.*, vol. 94, no. 15, p. 151 106, Apr. 2009.